

This accepted author manuscript of article: Eper-Pápai, I., Mentés, Gy. Comparison of two extensometric stations in Hungary

is copyrighted and published by Elsevier. It is posted here by agreement between Elsevier and MTA.

The definitive version of the text was subsequently published in: Geodynamics, 2014, Volume 80, pp. 3-11, October 2014, ISSN: 0264-3707.

DOI: <http://dx.doi.org/10.1016/j.jog.2014.02.007>

Available under license CC-BY-NC-ND.

1 **Comparison of two extensometric stations in Hungary**

2 Ildikó Eper-Pápai^a, Gyula Mentés^{a,*}, Márta Kis^b, András Koppán^b

3 ^aGeodetic and Geophysical Institute, Research Centre for Astronomy and Earth Sciences,

4 Hungarian Academy of Sciences, Csatkai E. u. 6–8, 9400 Sopron, Hungary. E-mail:

5 papai@ggki.hu, Phone: +36 99 508368, E-mail: mentes@ggki.hu, Phone: +36 99 508348

6 ^bGeological and Geophysical Institute of Hungary, Stefánia u.14, 1143 Budapest, Hungary.

7 E-mail: kis.marta@mfgi.hu, koppan.andras@mfgi.hu, Phone: +36 1 3843302

8 *Corresponding author E-mail address (Gy. Mentés): mentes@ggki.hu

9 Phone: +36 99 508348

10

11 **Abstract**

12 Quartz-tube extensometers are used to measure rock deformations in two geodynamic

13 observatories in Hungary in order to contribute to the investigation of recent tectonic

14 movements on the area of the Pannonian Basin. One of the observatories is situated on the

15 border of the Alps at Sopronbánfalva and is set in the metamorphic (gneiss) material of the

16 mountains. The other station is in the basically karstic environment of the Mátyáshegy

17 (Mátyás Hill) near Budapest. The aim of this paper is to investigate how the local conditions,

18 such as structure of the observatory, topography or geologic features of the surrounding rocks,

19 lead to additional or modified deformations of the extensometric stations. Data collected over

20 eight years were processed and analysed to compare the observatories taking into account

21 geologic, lithologic and topographic properties of the measurement sites. Tidal and coherence

22 analysis of the continuous strain measurements revealed that the instrument at Sopronbánfalva

23 is more sensitive to atmospheric pressure loading than the extensometer at Mátyáshegy.

24 Signal to noise values from the data processing of the short period variations support the

25 higher stability of tidal strain measurements at Mátyáshegy. The strain rates measured by

26 extensometers in both observatories are in good agreement with the strain rates inferred from
27 GPS measurements of the Hungarian GPS Geodynamic Reference Network and the Central
28 European GPS Reference Network.

29 Keywords: Earth tides; Extensometer; Barometric pressure; Geodynamic observatory; Strain
30 rate

31 **1. Introduction**

32 Extensometric measurements provide horizontal deformation data which incorporates the
33 short period tidal variations as well as local tectonic deformations in the long run, but the
34 recorded data are influenced by different effects depending on the local conditions of the
35 measurement site. Many publications deal with the influence of the construction and the
36 surroundings of the instrument's site appearing as cavity, topographic and lithologic effects
37 (e.g., Harrison, 1976; Brimich et al., 1998; Gebauer et al., 2009). Other works have been
38 published on the effect of atmospheric pressure loading on horizontal deformation
39 measurements (e.g., Müller and Zürn, 1983; Dal Moro and Zadro, 1998; Kroner et al., 2005;
40 Steffen et al., 2006; Zürn et al., 2007) under the conditions at a given measurement site and a
41 given type of measurement device.

42 In Hungary two observatories were established for seismic and gravity measurements and for
43 observation of tectonic movements and tides of the solid Earth: the Mátyáshegy Gravity and
44 Geodynamic Observatory (MGGO) in Budapest in a cave in Mátyáshegy and the
45 Sopronbánfalva Geodynamical Observatory (SGO) in Sopronbánfalva in an artificial gallery
46 (Fig. 1). In the MGGO two extensometers were installed in 1981 and 1985 (Latinina et al.,
47 1984) and in the SGO one extensometer in 1990. All instruments are quartz-tube
48 extensometers with capacitive transducers. Their construction and calibration are described in
49 detail by Mentés (2010). Since the measuring instruments are of the same type and capability
50 to monitor deformations, it is a good opportunity to compare two geodynamic observatories

51 which lie in different geologic, topographic and tectonic environments. Features of the
52 geodynamic deformation measurements at both sites in the high and low frequency ranges of
53 the signals are presented in this paper.

54 **2. Observation sites**

55 **2.1. Sopronbánfalva Geodynamic Observatory**

56 The Sopronbánfalva Geodynamic Observatory is located on the Hungarian-Austrian border in
57 the Sopron Mountains. The area belongs to the extensions of the Eastern Alps (Alpokalja
58 region), which extend eastward to the Rába fault (Fig. 1) regarded as the easternmost
59 termination of the Alps in Hungary. The crystalline rocks of the Alpokalja region crop out in
60 an area of 40 km² and are composed of folded, medium grade crystalline shists and
61 subordinate low-grade tectonites (muscovite gneiss and leucophyllite). The crystalline
62 basement of the mountains is covered by Neogene sediments. The Sopron Mountains consist
63 of metamorphic rocks of Palaeozoic age such as gneiss and different mica schists (Haas,
64 2001). The geological map of the surroundings of the observatory can be seen in Fig. 2. The
65 observatory is an artificial gallery driven into an outcrop of the muscovite gneiss which
66 belongs to the most schistose variety of the medium-grained gneisses called ‘Sopron type
67 gneisses’ (Kisházi and Ivancsics, 1985). The rock cover above of the observatory is about 60
68 m. There are no fractures and faults in the vicinity of the observatory. The yearly mean value
69 of the temperature is 10.4 °C in the gallery and the yearly and daily temperature variations are
70 less than 0.5 °C and 0.05 °C, respectively. The relative humidity is 90% and it is nearly
71 constant. The gallery where the extensometer is placed is thermally insulated but not perfectly
72 hermetically sealed. It means that there is a slow air circulation via the duct for the electric
73 cables of the instruments. This ventilation does not change the temperature in the gallery and
74 the instrument is not directly sensitive to air pressure variations (Mentes, 2000). The
75 coordinates of the SGO and the length and azimuth of the extensometer are given in Table 1.

76 The ground plane of the observatory and the location of the extensometer, which is nearly
77 perpendicular to the rock wall are shown in Fig. 3.

78 **2.2. Mátyáshegy Gravity and Geodynamic Observatory**

79 The Mátyáshegy Gravity and Geodynamic Observatory is situated in the karstic environment
80 of Mátyáshegy in the north-western suburban part of Budapest. The Mátyáshegy is a part of
81 the Buda Mountains, in north central Hungary, belonging to the regional unit ‘Transdanubian
82 Mountains’ (Fig. 1). The karstic cave system of the hill is the longest (13.465 km) exposed
83 cave system of West Hungary. The galleries were created by thermal water from the upper
84 Triassic flinty limestone and the discordantly bedding marine upper Eocene nummulitic
85 limestone. These formations are parts of the karstic water reservoir of the hydrology of this
86 area. The highest parts of the cavity reach up into the concordant bryozoan Marl. The tunnels
87 and galleries of the observatory were based on the natural cave system and were artificially
88 formed, mainly in the upper Eocene nummulitic limestone formation. Fig. 4 shows the
89 topographic map of the surroundings of the observatory and its entrance in the area of the
90 quarry located on the south-western side of the hill. The ground plane of the observatory with
91 the long (E1) and short (E2) extensometers is shown in Fig. 5. The galleries run under about
92 30 m of rock cover; the temperature variation in the inner galleries is less than 0.2 °C over a
93 year. The level of the karstic water is about a hundred meters deeper than the level of the
94 station. The River Danube flows about 2 km away from the observatory.

95 **3. Method**

96 Extensometric data recorded between 2005 and 2012 were used for calculations and for
97 comparison of the measurement sites. In both cases the sampling rate is one minute. High
98 frequency noises (well above the tidal range) are removed by built-in electric filters. Step and
99 spike disturbances were corrected and gaps in the data series were filled with adjusted
100 theoretical values in the course of preprocessing. The volume of the gaps is below 3 % per a

101 year at SGO and about 10 % for E2 at MGGO. However, the rate of the missing data was also
102 3 % for E2 in 2012. Continuous operation of E1 extensometer was interrupted for periods of
103 many months due to technical problems in 2011 and 2012. The signals were finally sampled
104 to one data/hour rate.

105 Features and transfer characteristics of the deformation measurements in the short-term band
106 of variations were examined by means of tidal analysis. Calculations were completed by the
107 ETERNA 3.40 Earth tide data processing package (Wenzel, 1996), using the Wahr-Dehant
108 Earth model (Wahr, 1981; Dehant, 1987) and the HW95 tidal potential catalogue (Hartmann
109 and Wenzel, 1995). A built-in high-pass filter of the program package (with a cut-off
110 frequency of 0.8 cpd) was used during the tidal evaluation. The residual strain data of the tidal
111 analysis were subjected to a Fourier transformation. The signal transfer properties of the two
112 stations were compared by tidal and coherence analyses. The admittances between strain and
113 the outer temperature were determined by a simple linear regression method. Coherence
114 analysis between theoretical and measured tide was used to investigate the transfer function of
115 the observatories (Formenti, 1999).

116 **4. Results**

117 **4.1. Tidal analysis**

118 A data series collected over eight years of the extensometer (SE) in the SGO (Fig. 3) and of
119 the extensometers E1 and E2 in the MGGO (Fig. 5) were subjected to tidal analysis
120 decomposing the data into one year segments. Evaluation of the data measured by
121 extensometer E1 – which resulted in highly distorted tidal parameters – was left out of the
122 investigation. Since the systematic checking and yearly calibration of the E1 extensometer
123 show proper functioning of the instrument in all other respects, the disturbed transfer
124 characteristics of the tidal signals is probably due to the relative position of the extensometer
125 to the gallery system of the observatory (see Fig. 5). The value of the tidal parameters from

126 analysis varies between 2–5 % at both measurement sites in the consecutive years, so data
127 processing of 2012 represents the multi-year measurement period. Adjusted tidal amplitudes
128 and the amplitude factors (measured/theoretical amplitudes) along with the standard
129 deviations of the adjustment for each component are listed in Table 2. The most striking
130 difference is the reduced diurnal amplitudes in the SGO. The main measured amplitudes are
131 44-60 % of the theoretical tidal deformation values. At the same time the S2 component in the
132 semidiurnal band is higher by a factor of 1.5 than it should be. Reduced amplitudes of E2 are
133 also adjusted in the diurnal band, which is similar to the SE results, but the differences
134 between the measured and theoretical values are much smaller. The most conspicuous
135 difference appears here in the K1 diurnal amplitude which decreased 25 %.

136 Since atmospheric pressure variations are among the main loading factors which affect the
137 deformation measurements at almost all kind of measurement sites (e. g. Rabbel and Zschau,
138 1985; Sun et al., 1995; Onoue and Takemoto , 1998; Kroner et al., 2005), pressure data series
139 measured in the observatories were taken into account and included in the tidal analysis. Data
140 processing results are presented in Table 2. In Fig. 6 the adjusted tidal amplitudes from the
141 analysis procedures can easily be compared. At Sopronbánfalva the linear regression
142 correction of the strain data by air pressure yielded an increase of about 5–10 % in the diurnal
143 band, while there is a more prominent decrease of 40 % at the S2 component, due to which
144 the S2 amplitude significantly improved compared to the theoretical value. From the
145 Mátyáshegy E2 data the analysis of the pressure-effect corrected extensometric series resulted
146 in insignificant, maximum 2 %, amplitude variations. This difference in the pressure
147 correction results are reflected also by the pressure sensitivity of the observatories, i.e. 4.5 nstr
148 hPa^{-1} in the SGO is against the value of the coefficient of 0.5 nstr/hPa in the MGGO. If the
149 deformation records are corrected for barometric pressure applying the above correction
150 factors in the time domain, the standard deviation of the residual signals (which are the

151 theoretical tides subtracted from the measured data) decrease from 6.1 to 5.1 nstr at the SGO
152 and from 2.6 to 2.5 nstr at the MGGO due to the correction.

153 The noticeable difference in the effect of atmospheric pressure variations at the two
154 measurement sites is demonstrated in Fig. 7. Here the residual of the high-pass filtered strain
155 data, which is provided by ETERNA among the analysis results, were subjected to a Fourier
156 transformation. Fast Fourier Transformation amplitudes of the residuals – after uncorrected
157 strain and pressure corrected strain analyses – are compared for both observatories in the tidal
158 frequency band (0-2.5 cpd). In the Sopronbánfalva data, an apparent decrease of the residual
159 amplitudes can be seen, especially in the 1 cpd band, while in Mátyáshegy amplitude changes
160 can hardly be noticed. The effect of the barometric pressure correction is characterised also by
161 numerical values: the average standard deviations of the tidal amplitudes (Table 2) and the
162 average spectral noise of the residual amplitudes (Fig. 7) decreased in the 1 cpd band (0.8–1.2
163 cpd) by 41 % at Sopronbánfalva and 4 % at Mátyáshegy, while in the 2 cpd band (1.8–2.2
164 cpd) by 22 % at Sopronbánfalva and below 1 % at Mátyáshegy. The values from the different
165 calculation methods agree with each other within 1 % in 1 cpd and 2 % in 2 cpd bands.

166 Overall characteristic of the tidal parameter determination at the investigated observatories is
167 concluded from Table 2. The determination is twice as accurate at the MGGO than it is at the
168 SGO for the comparison of the standard deviations of amplitude values for the main waves,
169 and of the standard deviations of weight unit of the adjustments. It matches the outcome of the
170 pressure correction of the data.

171 **4.2. Coherence analysis**

172 The two observatories were tested also by coherence analysis to determine how they transfer
173 the tidal signal. The coherence was calculated between theoretical and measured strain tide as
174 input and output signals of the Earth–observatory–system. The transfer function of the system
175 can be seen in Fig. 8. At the SGO the coherence is better than 0.95 in the semidiurnal band,

176 while in the diurnal band it is about 0.8. At the MGGO the coherence values are better than in
177 the SGO which means that the transfer of the tidal signal is less damped than at the SGO.

178 **4.3. Long term variations**

179 Deformation measurement data collected over eight years from the two observatories were
180 investigated. The recorded strain data of the Sopronbánfalva extensometer are drawn in Fig. 9
181 and curves of the E1 and E2 extensometers in the Mátyáshegy Observatory can be seen in
182 Figs. 10 and 11. The long-term variations are approximated in the Figures by linear trend lines
183 fitted to each data series along the recording period 2005–2012. The steepness of the trend
184 lines is the average strain rate in the investigated period. The measured strain rates are
185 summarised in Table 3 which also contains the strain rates measured in the MGGO by Varga
186 and Varga (1994) between 1990 and 1992. The peak to peak magnitudes of the yearly rock
187 strain variations caused mainly by the outer temperature variations (Mentes, 2000) –
188 determined after removing the trend from the curves – and the admittances between strain and
189 the outer temperature are listed in Table 3. This yearly period at SE and E1 clearly appears in
190 Figs. 9 and 10, while it is inconspicuous in the record of E2 (Fig. 11). The jumps and steep
191 changes in the strain records of the MGGO (Figs. 10 and 11) can be in connection with the
192 karstic water level changes under the observatory (Varga and Varga, 1994).

193 **5. Discussion**

194 Tidal analysis results reveal that the Mátyáshegy E2 instrument has a better capability to
195 transfer data of the horizontal high frequency deformations than the extensometer in the SGO.
196 Different behaviour of the extensometers due to atmospheric pressure loading can be
197 disclosed if the pressure parameter is included in the tidal analysis and the strain data is
198 corrected by a simple linear regression. Almost one order of magnitude higher regression
199 value resulted for SGO ($4.5 \text{ nstr hPa}^{-1}$) than for MGGO ($0.5 \text{ nstr hPa}^{-1}$). At the SGO a

200 significant improvement of the tidal adjustment resulted, while in Mátyáshegy the effect is not
201 detectable.

202 Beyond the similar instrument construction and the similar length of the galleries where the
203 instruments are placed, the overlaying topography of the measurement sites is also similar. At
204 the same time the rock coverage over the extensometers is two times higher at Soprobánfalva
205 than at Mátyáshegy, the gallery system of the MGGO is much more complex – due to the
206 original dissolved cave forms – than that of the SGO and a major difference exists in the
207 azimuths of the instruments. From point of the modifying cavity effect – being one of the
208 main site factors to be taken into consideration – a finite element model calculation resulted in
209 an 8 % increase of tidal rock deformation at the MGGO site. Such model calculations are not
210 at our disposal for the SGO, though from the literature the order of the disturbing cavity effect
211 for tidal strain, depending on the measurement arrangement and geometry, is about 1–10 %
212 (Harrison,1976; Sato and Harrison 1990). Thus, since the highest distortion of tidal
213 amplitudes in the SGO varies between 40–60 %, this correction item cannot be resolved here.
214 Lithologic parameters of the surrounding rocks at the measurement sites which describe the
215 different rock materials are listed in Table 4. On the basis of the model calculations of
216 Gebauer et al. (2009, 2010), where the cavity, topographic and lithologic effect on horizontal
217 deformations under atmospheric pressure load were investigated, the results of their
218 conclusions can be applied to these observatories in the increasing order of the magnitude of
219 the effect:

220 – The extent of the cavity effect for the lithologies of these observatories is about 0.1 nstr
221 hPa⁻¹, it is too small to be comparable with the difference in atmospheric pressure load effect
222 between SGO and MGGO. At the same time the galleries of SE and E2 are of almost the same
223 size and length.

224 – Since the rock cover above the instruments is different, a 20–30 % increase in the effect of
225 topography can be supposed at Sopronbánfalva (60 m) compared to Mátyáshegy (30 m), but
226 similarly to the previous effect its magnitude is small (below $0.5 \text{ nstr hPa}^{-1}$) and it may
227 explain only a minor part of the difference.

228 – From model calculations, a difference in the deformation effects in the order of about 2–2.5
229 nstr hPa^{-1} derives from the observatories having different rock material parameters and this
230 value much better approaches the difference of the pressure effects which were provided by
231 tidal analysis.

232 The above mentioned pressure load effects are related to a uniform pressure load condition.
233 Dynamic loading cases are also incorporated in the finite element modelling of Gebauer et al.
234 (2009, 2010). Since at Sopronbánfalva the gallery of the extensometer is parallel and at
235 Mátyáshegy the gallery of E2 is almost perpendicular to the prevailing wind direction, which
236 is the same above the regions of the observatories, the significantly higher pressure effect is in
237 good agreement with the modelling results.

238 On the basis of eight years of measurements it seems that two extensometers (SE and E1)
239 with almost the same azimuth, though far away from each other geographically, behave
240 similarly in the sense of yearly deformation changes. Nevertheless the different yearly
241 amplitudes should be noticed. The similarity between the conditions of the instruments is the
242 position of the galleries (where they are placed) relative to the topography of the surface
243 forms, the steep scarps, of the observatories. However, the Mátyáshegy Observatory has a
244 cave system while at Sopronbánfalva the galleries were made only for the instruments. This
245 complex gallery system of the MGGO leads to the different transfer mechanism induced by
246 temperature variations in the case of E1 and E2 (Figs. 10 and 11). Due to their free
247 unhindered deformation, the rock walls between the galleries in the MGGO absorb a part of
248 the deformation energy caused by barometric pressure and temperature variations. This can

249 explain the lower pressure admittance and temperature induced peak to peak yearly strain
250 variations in the MGGO compared to SGO (Table 3).

251 The highest rate of the long-term deformation changes at Sopronbánfalva can be attributed to
252 the geographical location of the instrument. The area belongs to the marginal mountainous
253 region of the Pannonian Basin with mostly crystalline bedrock types, and this East Alpine
254 region is characterised by different vertical deformation velocities compared to the central
255 parts of the Pannonian Basin (Cloetingh et al., 2005; Caporali, 2009; Dombrádi et al., 2010).

256 The folding and compression of the weak lithosphere absorbs the strain in the Pannonian
257 Basin (Dombrádi et al., 2010) which explains the small strain rates measured in the
258 Mátyáshegy Observatory. Extensometer E2 is nearly parallel to the maximum horizontal
259 stress direction assumed by Bada et al. (2007a, b) and it measures a higher rate than E1 (Table
260 3) which lies almost perpendicular to the direction of E2. These local strain rates are in good
261 accordance with the strain rates measured by geodetic methods (see Table 3). The strain rates
262 determined from GPS measurements in the Hungarian GPS Geodynamic Reference Network
263 and the Central European GPS Reference Network (Grenerczy et al., 2000, 2005) are three
264 orders of magnitude smaller than the values measured by the extensometers. It can be
265 explained by the difference of the measurement techniques. While the extensometer measures
266 local strain rates, only global strain rates for large areas can be determined from GPS
267 measurements. The faults between GPS stations and earthquakes in the region release the
268 strain (Bada et al., 2007b; Bus et al., 2009). In the region of the SGO the strain rate measured
269 by GPS is twice the value obtained in Central Hungary. Varga et al. (2002) determined a
270 strain rate of $-0.08 \mu\text{str year}^{-1}$ from the Hungarian Triangulation Network in the Budapest
271 region, which is the same value measured by the E1 extensometer in the MMGO. Although
272 extensometric measurements are influenced by local tectonic processes (e.g., orogenic forces),
273 they describe the recent tectonic movements in the Pannonian Basin very well.

274 **7. Conclusions**

275 The uniform construction of the extensometers in the Mátyáshegy Gravity and Geodynamic
276 Observatory and in the Sopronbánfalva Geodynamic Observatory ensures that in the course of
277 comparison any differences in the measurement characteristics can be attributed to geologic,
278 topographic properties and meteorological conditions of the measurement sites.

279 Tidal analysis of the extensometric data between 2005 and 2012 revealed that the measured
280 tidal amplitudes are close to the theoretical values in the MGGO while they are 44-60 %
281 smaller in the diurnal band in the SGO. The difference in the tidal signals (also proved by
282 coherence analysis) can be attributed to the different barometric pressure sensitivity of the
283 observatories ($4.5 \text{ nstr hPa}^{-1}$ in the SGO and $0.5 \text{ nstr hPa}^{-1}$ in MGGO).

284 The results of the barometric pressure correction show that while in the MGGO a simple
285 regression correction yields good improvement of the signal-to-noise ratio in the strain data,
286 in the SGO a more sophisticated reduction method is needed which takes into account
287 regional and possibly global air pressure data to correct for the effect of passing weather
288 fronts.

289 The long-term thermal effect in the MGGO is about the half of the one in the SGO. The
290 difference between the pressure and thermal sensitivity of the observatories is due to the
291 different geologic, lithology parameters, gallery system and the position of the instrument
292 relative to the topography of the measurement sites.

293 In contrast with the different transfer characteristics of the observatories in the tidal domain
294 and the high long-term disturbances in the MGGO, probably caused by karstic water
295 variations, the measured strain rates are in good agreement with the GPS measurements in the
296 Hungarian GPS Geodynamic Reference Network and the Central European GPS Reference
297 Network.

298 The investigated geodynamic observatories and extensometers are parts of an extensometric
299 observatory network on the territory of the Pannonian Basin. Therefore the analysis results
300 may be utilized when the deformation measurements of the network are processed and the
301 specific sensitivity of the measurement locations can lead to satisfactory corrections both in
302 the high and low frequency ranges of the signals. It may contribute to a unified evaluation and
303 interpretation.

304 **Acknowledgements**

305 The authors are grateful to three anonymous reviewers for their valuable comments and
306 suggestions which helped to improve the paper. This work was funded by the Hungarian
307 National Research Fund (OTKA) under project No. K 109060. Special thanks to Tibor
308 Molnár for his careful maintenance of the instruments.

309 **References**

- 310 Bada, G., Grenerczy, Gy., Tóth, L., Horváth, F., Stein, S., Cloetingh, S., Windhoffer, G.,
311 Fodor, L., Pinter, N., Fejes, I., 2007a. Motion of Adria and ongoing inversion of the
312 Pannonian Basin: Seismicity, GPS velocities and stress transfer. In: Stein, S., Mazzotti, S.,
313 (Eds.), *Continental Intraplate Earthquakes: Science, Hazard, and Policy Issues*. Geological
314 Society of America Special Papers 425 (16), 243–262, <http://dx.doi.org/10.1130/2007.2425>.
315 Bada, G., Horváth, F., Dövényi, P., Szafián, P., Windhoffer, G., Clothing, S., 2007b. Present
316 day stress field and tectonic inversion in the Pannonian basin. *Global Planet. Change* 58, 165–
317 180.
- 318 Brimich, L., Kohút, I., Kostecký, P., 1998. Influence of the Cavity Effect on Tidal
319 Measurements. In: Ducarme, B., Paquet, P. (Eds.), *Proceedings of the 13th International*
320 *Symposium on Earth Tides*, pp. 397–412.
- 321 Budai, T., Gyalog, L. (Eds.), 2009. *Geological Map of Hungary for Tourists*. Geological
322 Institute of Hungary, Budapest.

323 Bus, Z., Grenerczy, Gy., Tóth, L., Mónus, P., 2009. Active crustal deformation in two
324 seismogenic zones of the Pannonian region – GPS versus seismological observations.
325 *Tectonophysics* 474, 343–352.

326 Caporali, A., 2009. Lithospheric flexure, uplift and expected horizontal strain rate in the
327 Pannonian Carpathian region. *Tectonophysics* 474, 337–342.

328 Cloetingh, S., Mañenco, L., Bada, G., Dinu, C., Mocanu, B., 2005. The evolution of the
329 Carpathians–Pannonian system: interaction between neotectonics, deep structure,
330 polyphase orogeny and sedimentary basins in a source to sink natural
331 laboratory. *Tectonophysics* 410, 1–14.

332 Dal Moro, G., Zadro, M., 1998. Subsurface deformations induced by rainfall and atmospheric
333 pressure: tilt/strain measurements in the NE Italy seismic area. *Earth Planet. Sci. Lett.* 164,
334 193–203.

335 Dehant, V., 1987. Tidal parameters for an unelastic Earth. *Phys. Earth Planet. Inter.* 49, 97–
336 116.

337 Dombrádi, E., Sokoutis, D., Bada, G., Cloetingh, S., Horváth, F., 2010. Modelling recent
338 deformation of the Pannonian lithosphere: Lithospheric folding and tectonic topography.
339 *Tectonophysics* 484, 103–118.

340 Formenti, D., 1999. What is the coherence function and how can it be used to find
341 measurement and test setup problems. *Sound and Vibration, Questions and Answers*, Sage
342 Technologies, Morgan and Hill, California, 2–3.

343 Gebauer, A., Kroner, C., Jahr, T., 2009. The influence of topographic and lithologic features
344 on horizontal deformations. *Geophys. J. Int.* 177, 586–602, [http://dx.doi.org/10.1111/j.1365-](http://dx.doi.org/10.1111/j.1365-246X.2009.04072.x)
345 [246X.2009.04072.x](http://dx.doi.org/10.1111/j.1365-246X.2009.04072.x).

346 Gebauer, A., Steffen, H., Kroner, C., Jahr, T., 2010. Finite element modelling of atmosphere
347 loading effects on strain, tilt and displacement at multi-sensor stations. *Geophys. J. Int.* 181,
348 1593–1612, <http://dx.doi.org/10.1111/j.1365-246X.2010.04549.x>.

349 Grenerczy, Gy., Kenyeres, A., Fejes, I., 2000. Present crustal movement and strain
350 distribution in Central Europe inferred from GPS measurements. *J. Geophys. Res.*
351 105 (B9), 21835–21846.

352 Grenerczy, Gy., Sella, G., Stein, S., Kenyeres, A., 2005. Tectonic implications of the
353 GPS velocity field in the northern Adriatic region. *Geophys. Res. Lett.* 32, L16311,
354 <http://dx.doi.org/10.1029/2005GL022947>.

355 Haas, J. (Ed.), 2001. *Geology of Hungary*. Eötvös University Press, Budapest, pp. 315.

356 Harrison, J.C., 1976. Cavity and topographic effects in tilt and strain measurements. *J.*
357 *Geophys. Res.* 81, 319–328.

358 Hartmann, T., Wenzel, H.G., 1995. The HW95 tidal potential catalogue. *Geophys. Res. Lett.*
359 22 (24), 3553–3556.

360 Kisházi, P., Ivancsics, J., 1985. Genetic petrology of the Sopron crystalline schist sequence.
361 *Acta Geol. Hu.* 28 (3–4), 191–213.

362 Kroner, C., Jahr, T., Kuhlmann, S., Fischer, K.D., 2005. Pressure induced noise on horizontal
363 seismometer and strainmeter records evaluated by finite element modelling. *Geophys. J. Int.*
364 161, 167-178, <http://dx.doi.org/10.1111/j.1365-246X.2005.02576.x>.

365 Latinina, L.A., Szabó, G., Varga, P., 1984. Observations of the deformation of the Earth's
366 crust in the Mátyáshegy cave near Budapest. *Acta Geod. Geophys. Mont. Hung.* 19, 197–205.

367 Mentés G., 2000. Influence of Temperature and Barometric Pressure Variations on
368 Extensometric Deformation Measurements at the Sopron Station. *Acta Geod. Geophys. Hung.*
369 35 (3), 277–282.

370 Mentés, Gy., 2010. Quartz tube extensometer for observation of Earth tides and local tectonic
371 deformations at the Sopronbánfalva Geodynamic Observatory, Hungary. *Rev. Sci. Instrum.*
372 81, 074501, <http://dx.doi.org/10.1063/1.3470100>.

373 Müller, T., Zürn, W., 1983. Observation of gravity changes during the passage of cold fronts.
374 *J. Geophys.* 53, 155–162.

375 Onoue, K., Takemoto, S., 1998. Atmospheric pressure effect on ground strain observation at
376 Donzurubo Observatory, Nara, Japan. In: Ducarme, B., Paquet, P. (Eds.), *Proceedings of the*
377 *13th International Symposium on Earth Tides*, pp. 157–164.

378 Rabbel, W., Zschau, J., 1985. Static deformations and gravity changes at the Earth's surface
379 due to atmospheric loading. *J. Geophys.* 56, 81–99.

380 Sato, T., Harrison, J.C., 1990. Local effects on tidal strain measurements at Esashi, Japan.
381 *Geophys. J. Int.* 102, 513–526.

382 Steffen, H., Kuhlmann, S., Jahr, T., Kroner, C., 2006. Numerical Modeling of the Barometric
383 Pressure-Induced Noise in Horizontal Components for the Observatories Moxa and Schiltach.
384 *J. Geodyn.* 41, 242–252.

385 Sun, H.P., Ducarme, B., Dehant, V., 1995. Effect of the atmospheric pressure on surface
386 displacement. *J. Geodesy* 70, 131–139.

387 Varga, P., Varga, T., 1994. Recent horizontal deformation in the Pannonian Basin measured
388 with extensometers. *Acta Geod. Geophys. Hung.* 29, 57–80.

389 Varga, P., Verbitskie, T.Z., Latinina, L.A., Brimich, L., Mentés, G., Szádeczky-Kardos, G.,
390 Eperne, P.I., Guseva, T.V., Ignatishin, V.V., 2002. Horizontal deformation of the Earth's crust
391 in the Carpathian region. (In Russian), *Science and Technology in Russia.* 58 (7) – 59 (1), 5–
392 8.

393 Wahr, J.M., 1981. Body tides on an elliptical, rotating, elastic and oceanless Earth. *Geophys.*
394 *J. R. Astr. Soc.* 64, 677–703.

395 Wenzel, H.G., 1996. The nanogal software: Earth tide data processing package ETERNA
396 3.30. Bull. d'Inf. Marées Terr. 124, 9425–9439.

397 Zürn, W., Exß, J., Steffen, H., Kroner, C., Jahr, T., Westerhaus, M., 2007. On reduction of
398 long-period horizontal seismic noise using local barometric pressure. Geophys. J. Int. 171,
399 780–796.

400

401 **Figure captions**

402 **Fig. 1.** Extensometric stations in Hungary.

403 **Fig. 2.** Geological map (Haas, 2001) of the surroundings of the SGO.

404 **Fig. 3.** Ground plane of the SGO with the instruments.

405 **Fig. 4.** Topographic map of the surroundings of the Mátyáshegy Observatory (Budai and
406 Gyalog, 2009).

407 **Fig. 5.** Ground plane of the MGGO with the instruments.

408 **Fig. 6.** Amplitudes of tidal components from ETERNA analysis of extensometric data from
409 Sopronbánfalva (SE) and Mátyáshegy (E2) observatories. U, C and T denote amplitudes from
410 analysing raw data, data corrected for barometric pressure by ETERNA and theoretical tide,
411 respectively.

412 **Fig. 7.** Fast Fourier Transformation amplitudes of tidal analysis residuals at the SGO and
413 MGGO. a) and c) residual amplitudes after strain analysis, b) and d) residual amplitudes after
414 local barometric pressure corrected strain analysis.

415 **Fig. 8.** Transfer characteristic (coherence function between the theoretical and measured
416 tides) of the Earth – observatory – instrument system at the SGO and at the MGGO.

417 **Fig. 9.** Extensometric raw data at the SGO from 1 Jan. 2005 to 31 Dec. 2012.

418 **Fig. 10.** Extensometric raw data measured by extensometer E1 at the MGGO from 1 Jan.
419 2005 to 31 Dec. 2012.

420 **Fig. 11.** Extensometric raw data measured by extensometer E2 at the MGGO from 1 Jan.
421 2005 to 31 Dec. 2012.

422

Figure1
[Click here to download high resolution image](#)

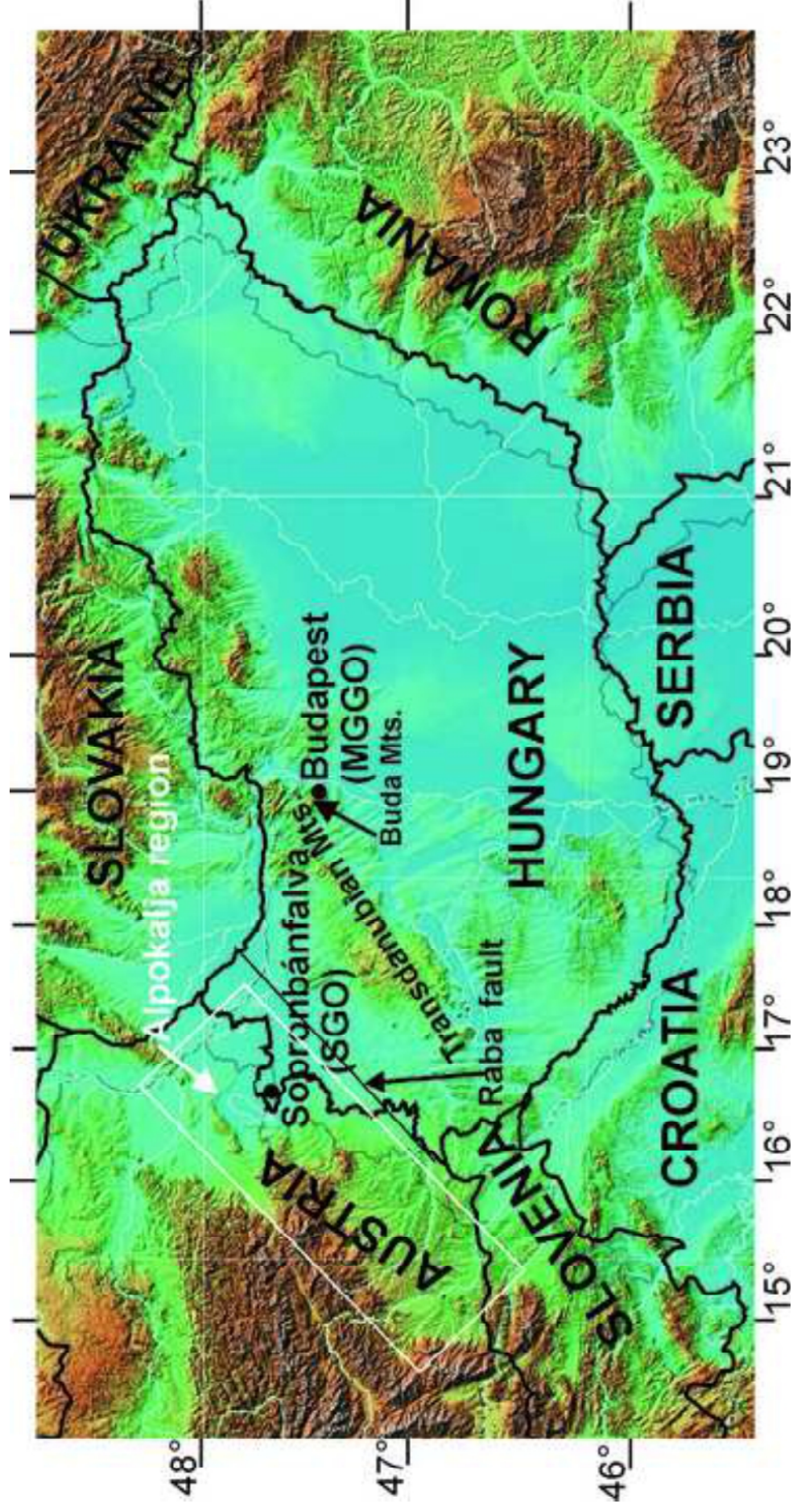
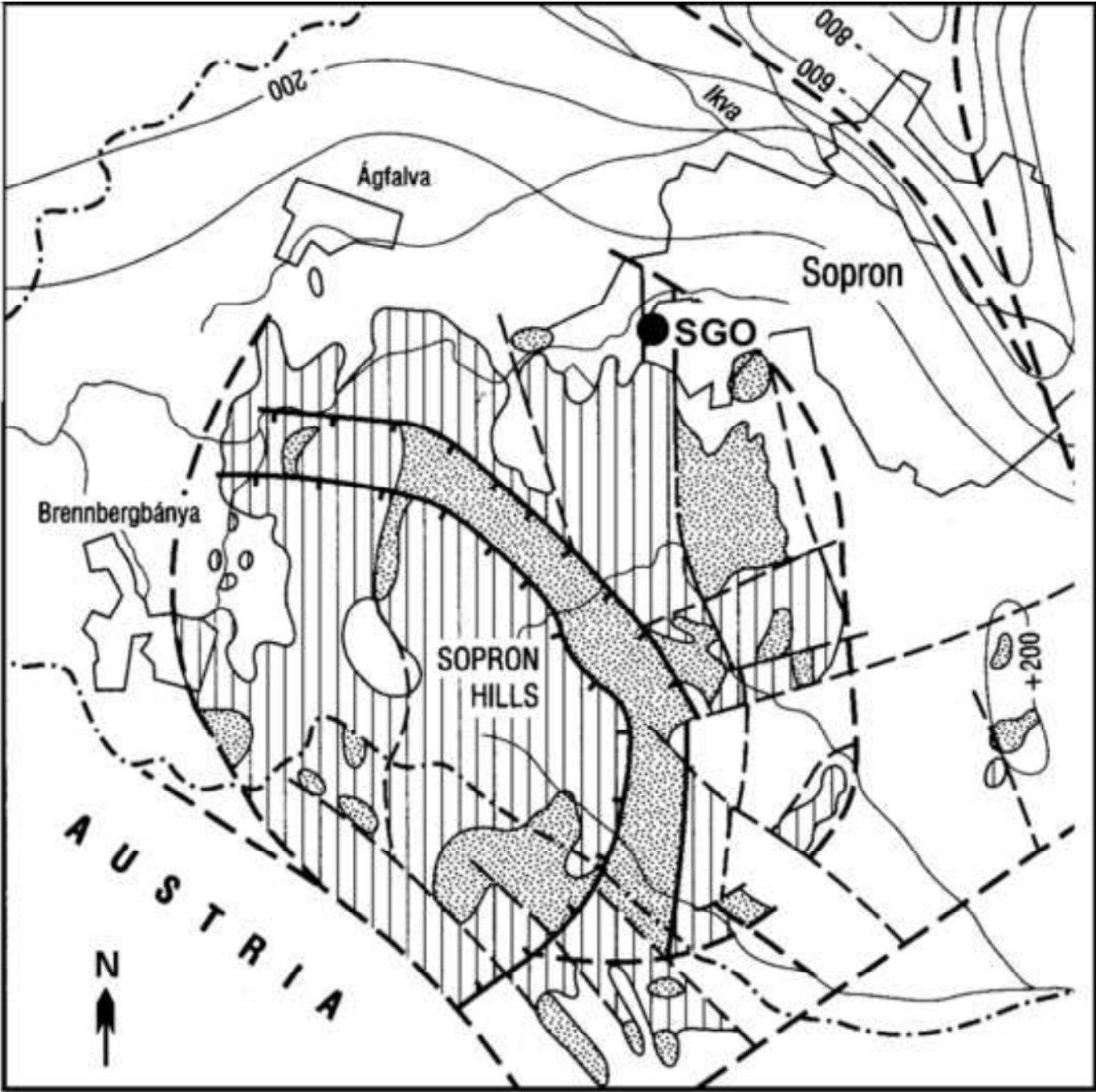


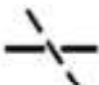




Figure2
[Click here to download high resolution image](#)



0 3 km

-  Sopron Gneiss Formations
-  Sopron Micaschist Formation

-  faults
-  scale boundary
-  nappe boundary

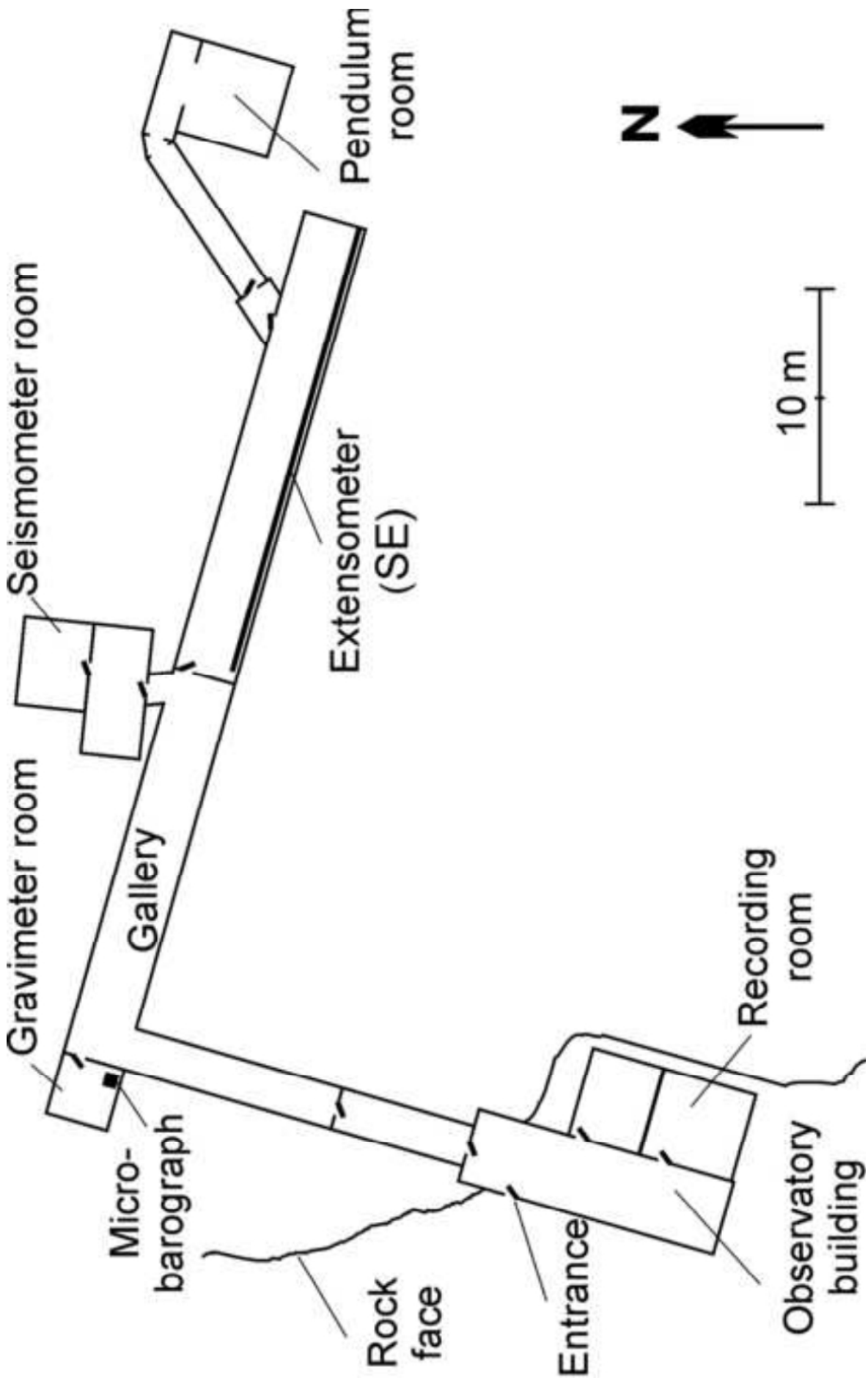


Figure3
[Click here to download high resolution image](#)

Figure4
[Click here to download high resolution image](#)

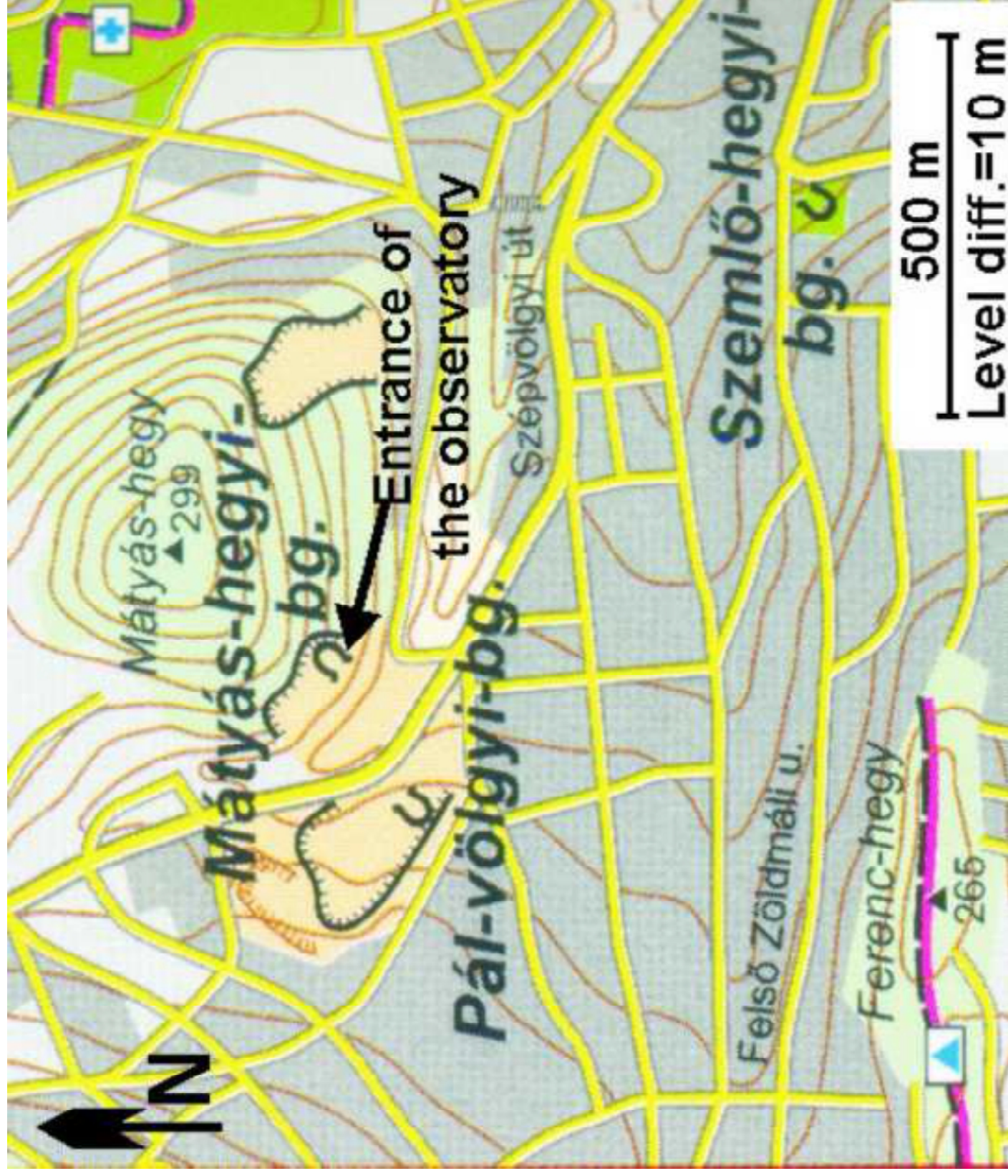


Figure5
[Click here to download high resolution image](#)

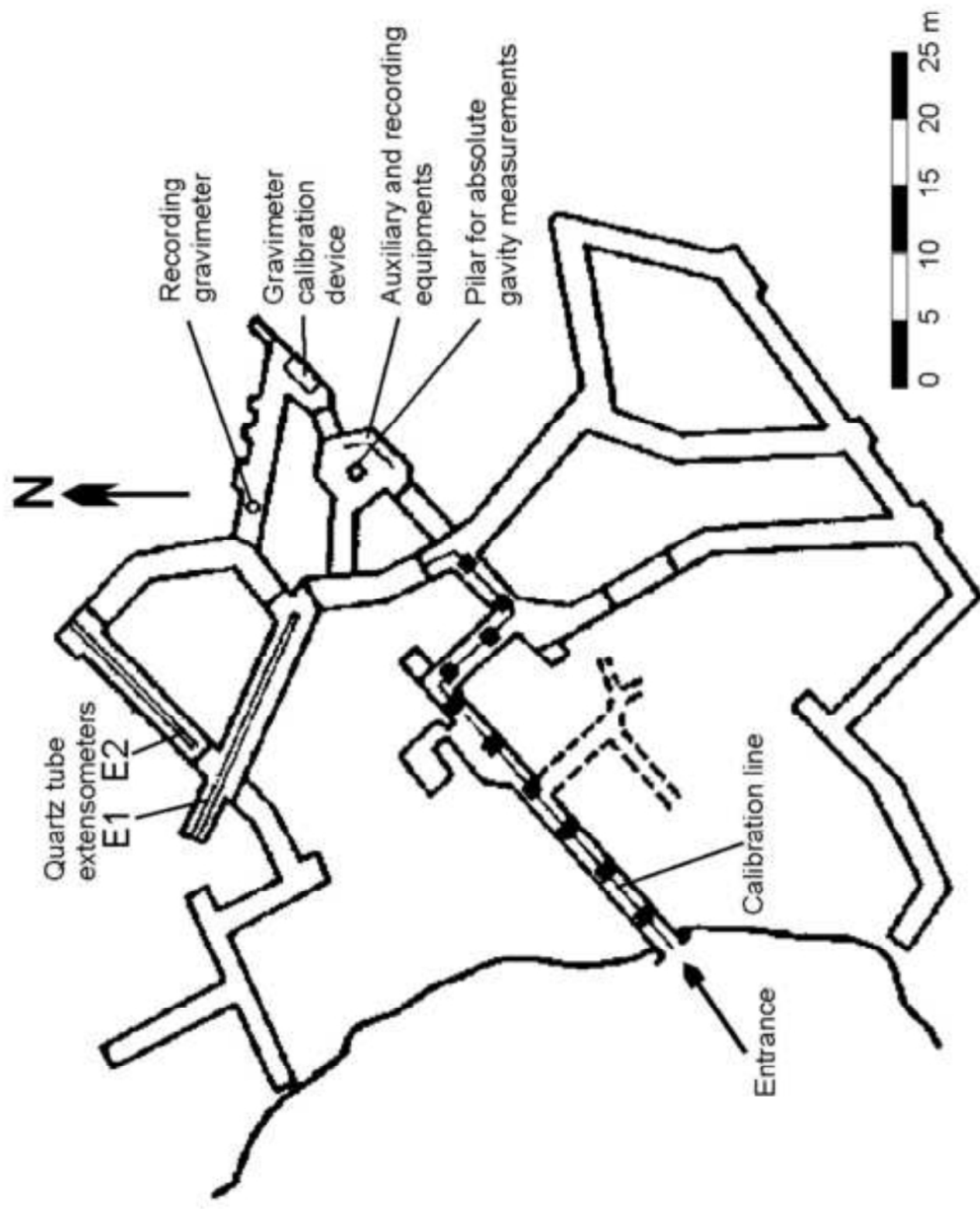


Figure6
[Click here to download high resolution image](#)

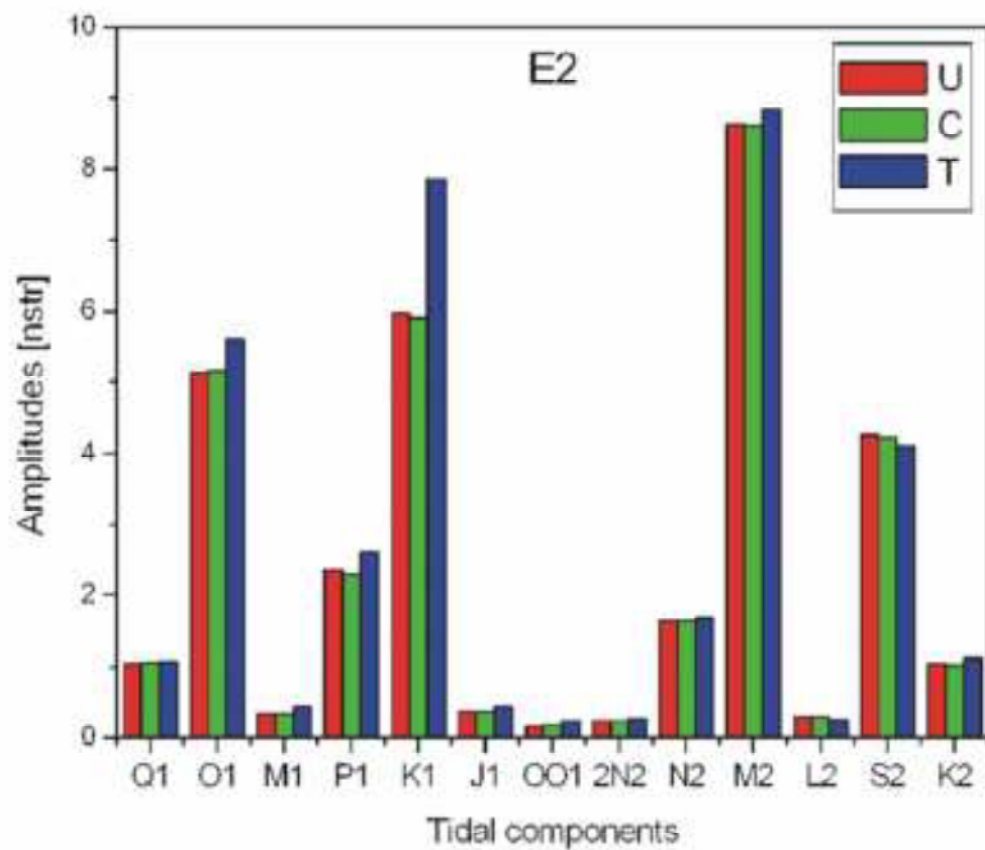
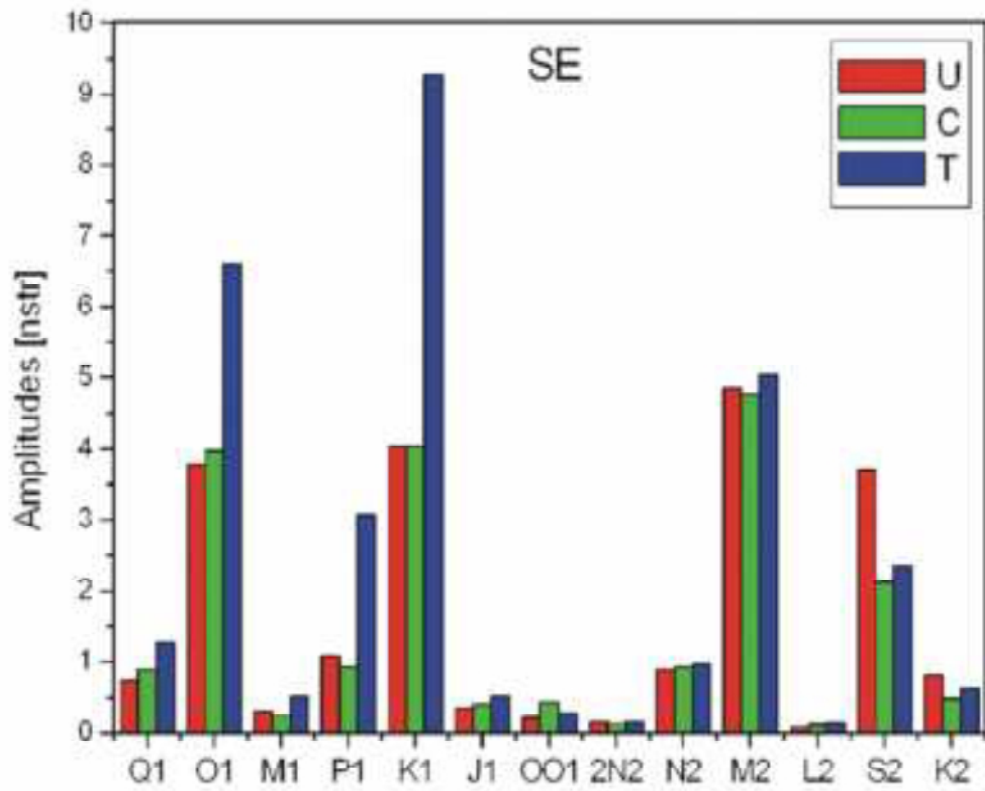
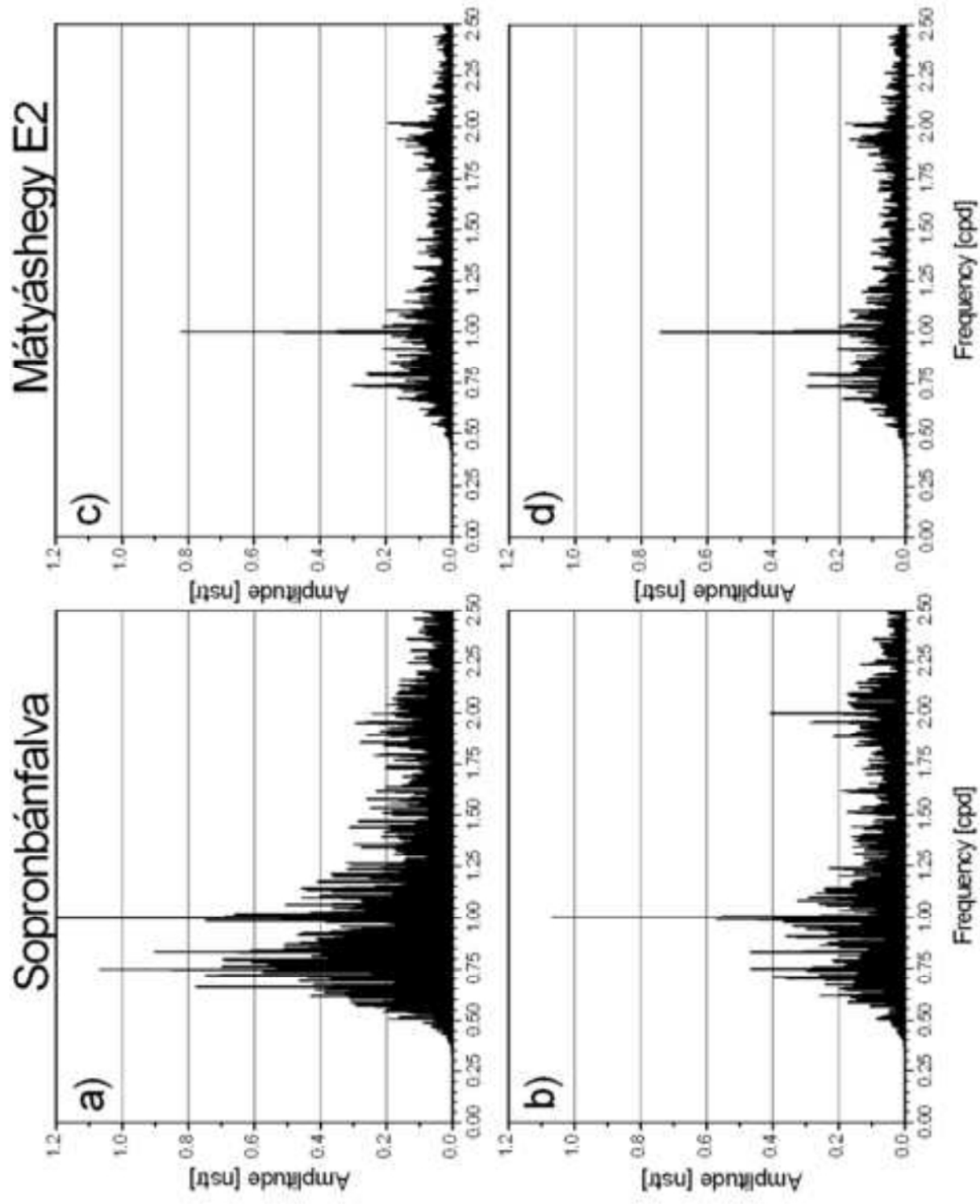


Figure7
[Click here to download high resolution image](#)



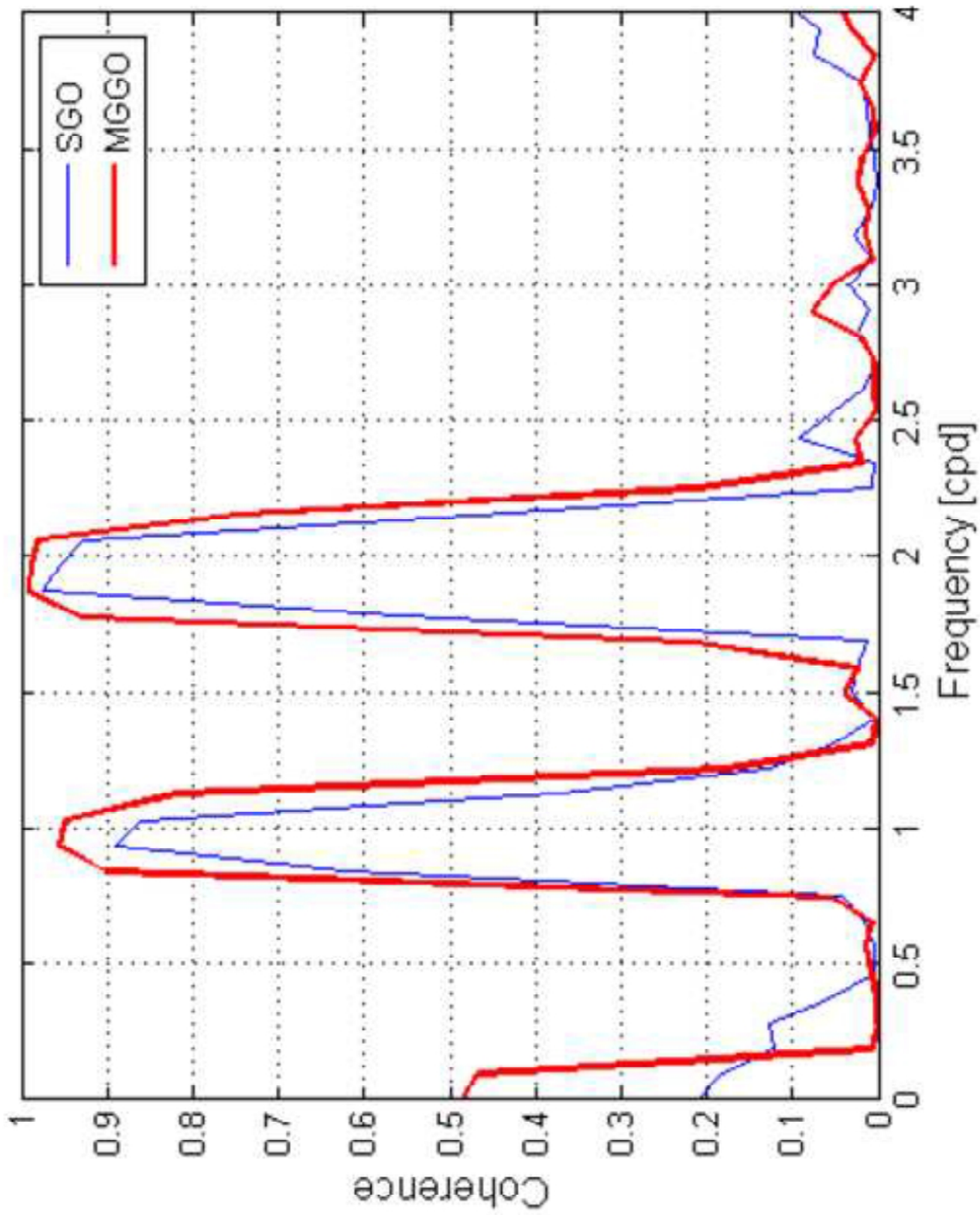


Figure8
[Click here to download high resolution image](#)

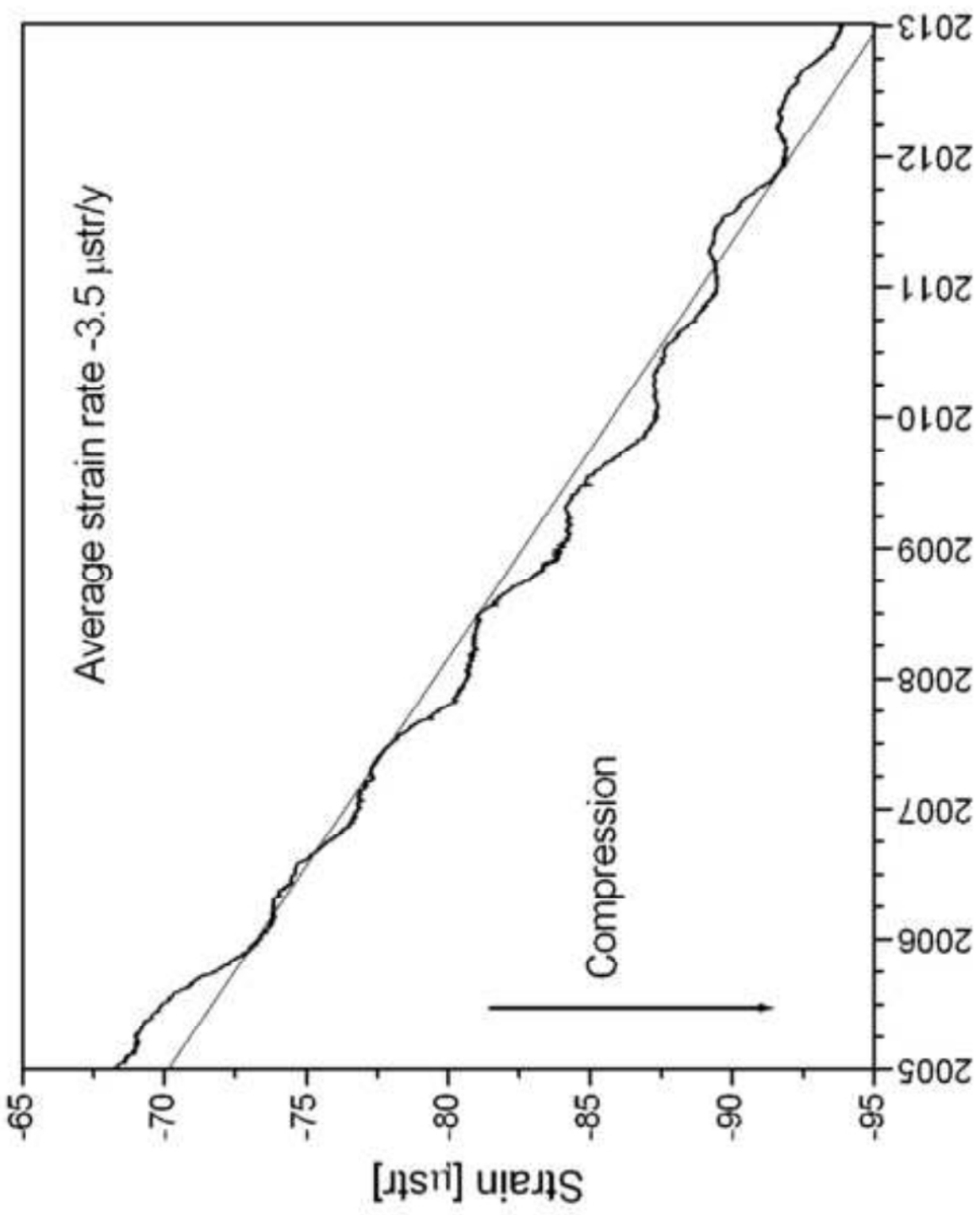


Figure9
[Click here to download high resolution image](#)

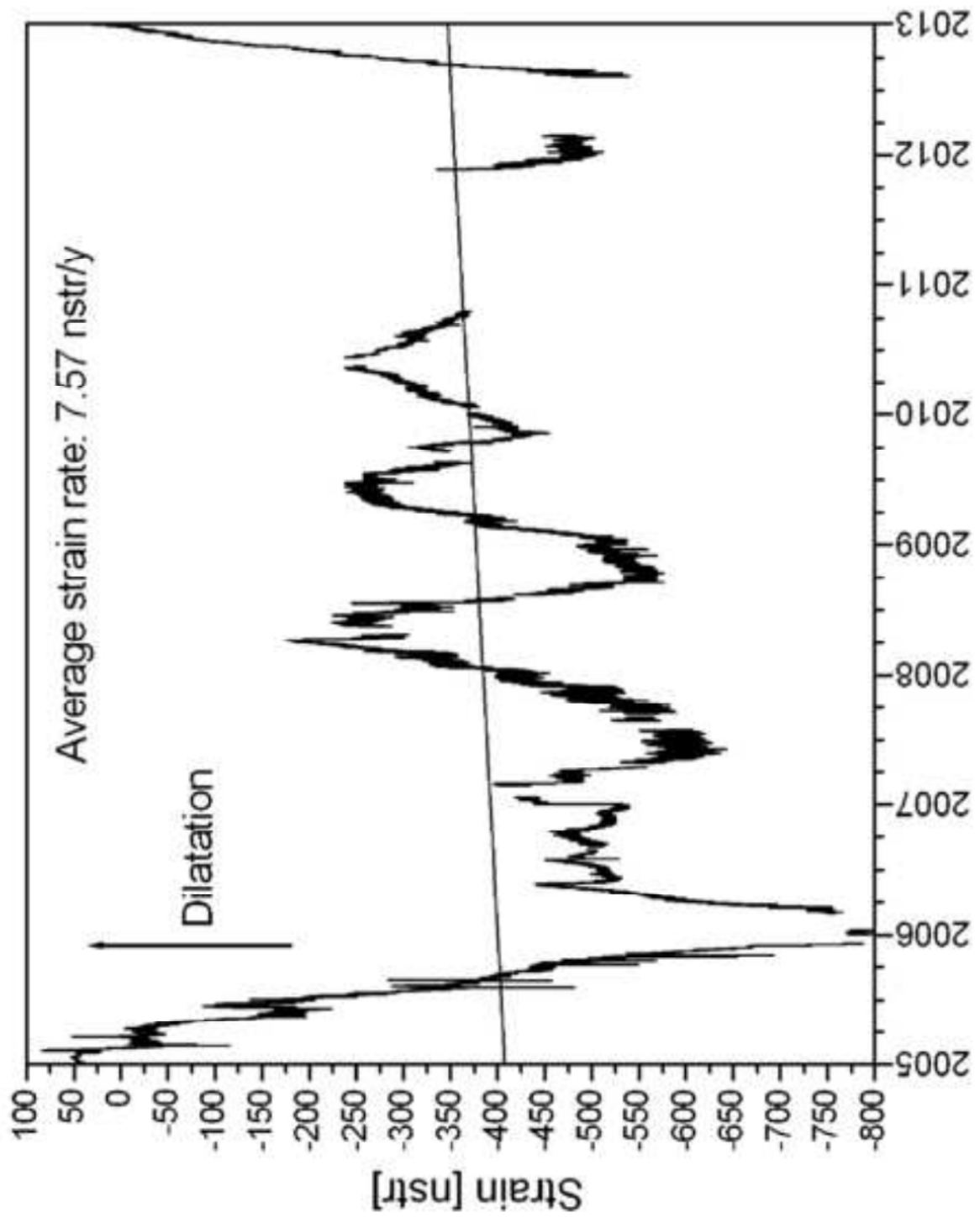


Figure10
[Click here to download high resolution image](#)

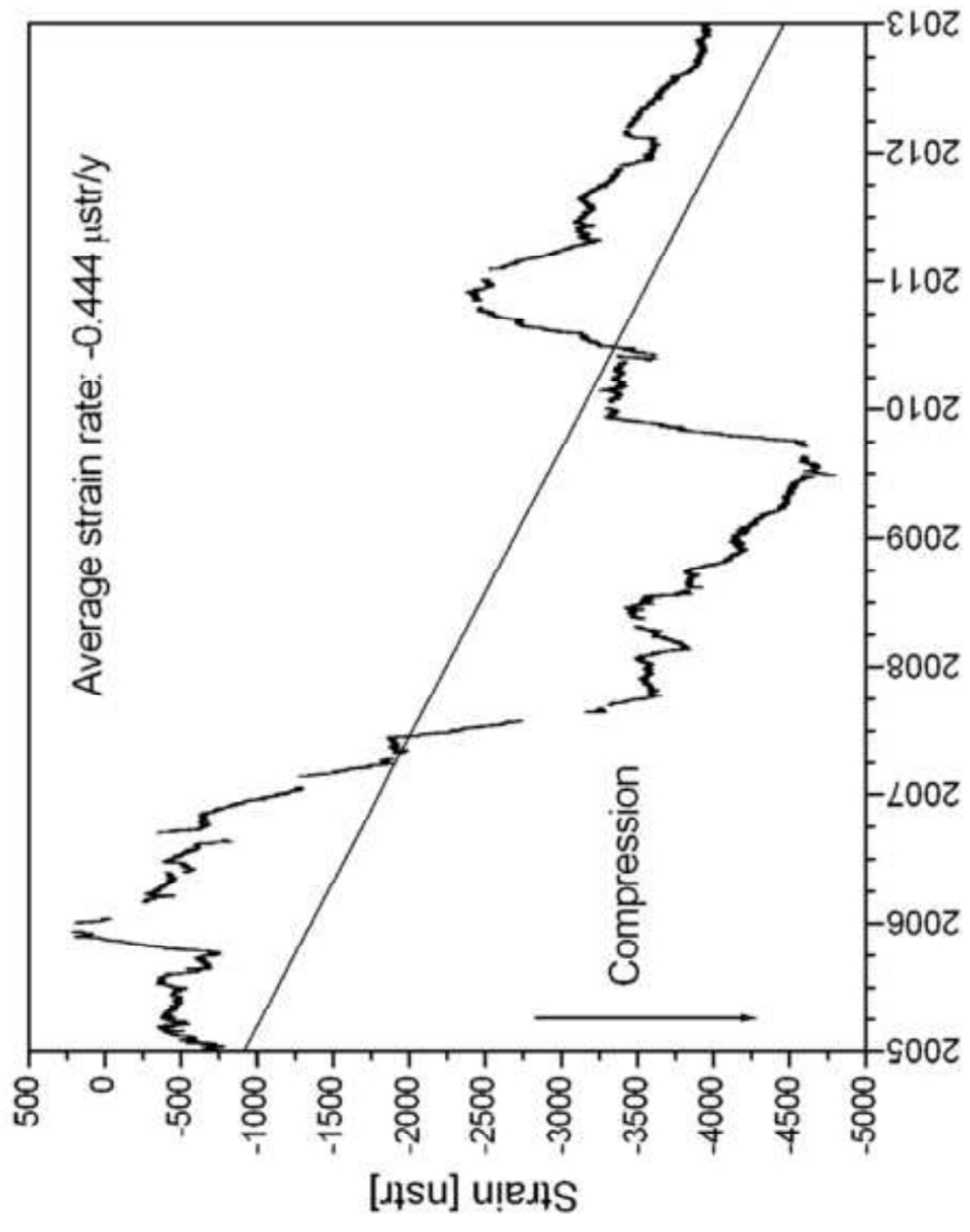


Figure11
[Click here to download high resolution image](#)

Table 1. Coordinates and parameters of the extensometers.

Extensometer	Coordinates of the station			Azimuth of the instrument	Length of the instrument [m]
	Latitude	Longitude	Height a.s.l. [m]		
Mátyáshegy E1	47° 33' 11"	19° 20' 24"	240	114°	21.3
Mátyáshegy E2	47° 33' 11"	19° 20' 24"	240	38°	13.8
Sopronbátfalva	47° 40' 55"	16° 33' 32"	220	116°	22

Table 2. Tidal analysis results of the deformation data recorded at the Sopronbánfalva Observatory and at the Mátyáshegy Observatory (extensometer E2) between 01 January 2012 and 31 December 2012.

Waves	Sopronbánfalva				Budapest E2			
	Analysis of uncorrected data		Analysis with pressure data		Analysis of uncorrected data		Analysis with pressure data	
	Amplitude±S.D.	factor±S.D.	Amplitude	Amplitude±S.D.	Amplitude±S.D.	Amplitude	Amplitude±S.D.	Amplitude
	[nstr]			[nstr]	[nstr]	factor±S.D.	[nstr]	factor±S.D.
Q1	0.752±0.247	0.596±0.196		0.891±0.145	1.048±0.085	0.977±0.080	1.051±0.082	0.980±0.077
O1	3.786±0.267	0.574±0.040	3.981±0.157	3.981±0.157	5.151±0.092	0.919±0.016	5.173±0.089	0.923±0.016
M1	0.306±0.282	0.591±0.543	0.238±0.165	0.238±0.165	0.341±0.097	0.774±0.219	0.341±0.093	0.774±0.211
P1	1.083±0.259	0.353±0.085	0.933±0.152	0.933±0.152	2.350±0.090	0.901±0.034	2.291±0.087	0.879±0.033
K1	4.041±0.271	0.436±0.029	4.048±0.159	4.048±0.159	5.986±0.094	0.760±0.012	5.918±0.091	0.751±0.012
J1	0.351±0.270	0.678±0.520	0.408±0.159	0.408±0.159	0.361±0.093	0.819±0.212	0.368±0.090	0.834±0.204
OO1	0.220±0.304	0.774±1.072	0.432±0.179	0.432±0.179	0.165±0.105	0.686±0.435	0.182±0.101	0.755±0.420
2N2	0.150±0.080	0.969±0.518	0.132±0.061	0.132±0.061	0.239±0.035	0.884±0.128	0.242±0.034	0.898±0.128
N2	0.889±0.105	0.918±0.109	0.927±0.081	0.927±0.081	1.631±0.046	0.964±0.027	1.634±0.046	0.966±0.027
M2	4.864±0.104	0.962±0.020	4.767±0.079	4.767±0.079	8.635±0.046	0.978±0.005	8.620±0.046	0.976±0.005
L2	0.085±0.081	0.594±0.564	0.119±0.062	0.119±0.062	0.286±0.035	1.146±0.140	0.292±0.035	1.169±0.139
S2	3.709±0.103	1.576±0.044	2.128±0.084	2.128±0.084	4.257±0.046	1.036±0.011	4.212±0.046	1.025±0.011
K2	0.813±0.115	1.272±0.181	0.487±0.089	0.487±0.089	1.050±0.051	0.941±0.046	1.030±0.051	0.923±0.046
S.D. of weight unit [nstr]	3.915		2.239		1.434		1.384	
Pressure regression coefficient [nstr/hPa]			4.5				0.5	

Table 3. Results of the long-term extensometric and geodetic measurements. (GPS SGO and GPS MGGO denote GPS measurements in the region of SGO and MGGO, respectively; HTN MGGO denote the strain rate determined from the Hungarian Triangulation Network in the region of the MGGO.)

Measuring method	Strain rate [$\mu\text{str year}^{-1}$]	Type of deformation	Admittance $\mu\text{str } ^\circ\text{C}^{-1}$	Annual peak to peak strain variation [μstr]	Measurement period
SGO E1	-3.5	compression	0.023	1	2005–2012
MGGO E1	0.0076	extension	0.009	0.4	2005–2012
MGGO E2	-0.444	compression	0.006	0.3	2005–2012
MGGO E1	-0.08	compression	–	–	1990–1992
MGGO E2	-2.24	compression	–	–	1990–1992
GPS SGO	-0.008	compression	–	–	1991–2007
GPS MGGO	-0.004	compression	–	–	1991–2007
HTN MGGO	-0.08	compression	–	–	1878–1965

Table 4. Lithologic parameters of the rock around the observatories

Observatory	Rock material	Density [kg m ⁻³]	Young's modulus [GPa]	Poisson ratio
Sopronbánfalva	Gneiss	2700	45.5	0.12
Mátyáshegy	Limestone	2500	65.0	0.25